Carbohydrate Polymers 118 (2015) 170–182

Contents lists available at ScienceDirect

Carbohydrate Polymers

journal homepage: www.elsevier.com/locate/carbpol

Amorphized cellulose as filler in biocomposites based on poly(ε-caprolactone)

M. Cocca [1], R. Avolio [1], G. Gentile *, E. Di Pace, M.E. Errico, M. Avella

Institute for Polymers, Composites and Biomaterials—National Research Council, Via Campi Flegrei 34, 80078 Pozzuoli, NA, Italy

ARTICLE INFO

Article history:
Received 18 September 2014
Received in revised form 23 October 2014
Accepted 5 November 2014
Available online 20 November 2014

Keywords:
Cellulose
Structure
Filler
Biocomposites
PCL

ABSTRACT

Amorphous cellulose particles, obtained through a solvent-free mechano-chemical process, have been tested for the first time as a potential filler for biodegradable composites based on poly(ε-caprolactone) (PCL). Commercial cellulose fibers have been also tested for comparison. An effective interfacial strategy based on a compatibilizing agent, a modified PCL, has been used to improve the polymer/filler interfacial adhesion. Composites have been tested through physico-mechanical characterizations and soil burial degradation tests, in order to evaluate the influence of cellulose structure and morphology and polymer/filler interfacial adhesion on the final properties of the realized materials. The use of the amorphous cellulose particles combined with the presence of a suitable interfacial agent has allowed to modulate relevant technological properties of the realized composites, such as tensile and thermal properties, water absorption, water vapor transmission rate and biodegradation kinetic.

1. Introduction

Durability properties are typical of traditional petroleum-derived polymeric materials and make them suitable for several applications. At the same time, these properties lead to relevant waste disposal problems because traditional polymers are resistant to microbial degradation and accumulate in the environment with an even growing landfilling rate (European Commission, 2013). In this view, biodegradable materials are considered as a potential solution to plastic littering. Therefore, the development of biodegradable plastics such as polylactide (PLA), poly(ε-caprolactone) (PCL), poly(hydroxyalkanoates) (PHA), poly(butylene succinate) (PBS) and their blends and composites have attracted an increasing scientific attention in order to reduce the extent of waste disposal problems (Nampoothiri, Nair, & John, 2010; Reddy, Ghai, Rashmi, & Kalia, 2003; Siracusa, Rocculi, Romani, & Dalla Rosa, 2008; Tian, Tang, Zhuang, Chen, & Jing, 2012).

Among these materials, in the last years systems based on biodegradable polyesters containing thermoplastic starch (Bastioli, 1998; Liu, Xie, Yu, Chen, & Li, 2009; Lu, Xiao, & Xu, 2009) have seen a constant industrial growth, despite to the debate on the non-food uses of agricultural resources (Tenenbaum, 2008). However, finding suitable cheaper alternative to thermoplastic starch for the production of biodegradable plastics is of relevant industrial interest (Wolf, 2010).

As concerning composites based on biodegradable matrices and reinforced with natural fibers, several research works have reported the results obtained by coupling ductile polyester matrices and different lignocellulosic fibers (Avella et al., 2007, 2008; Bogoeva-Gaceva et al., 2007; Buzarovska et al., 2007; Dimzoski et al., 2008; Faruk, Bledzki, Fink, & Sain, 2012; John & Thomas, 2008; Satyanarayana, Arizaga, & Wypych, 2009). Other systems are based on the use of non fibrous natural fillers, such as wood flour (Dányádi et al., 2007; Dominkovics, Dányádi, & Pukánszky, 2007; Faludi, Dora, Renner, Móczó, & Pukánszky, 2013). In most cases the main drawback of all these materials, in comparison to starch based blends, is the significant decrease of the elongation at break even at low fiber loading (Cyras, Iannace, Kenny, & Vasquez, 2001; Ganster & Fink, 2006; Joseph & Thomas, 1996; Keller, 2003; Nestore, Kajaks, Vancovicha, & Reihmane, 2013; Wollerdorfer & Bader, 1998), independently of the strategy adopted to improve the filler/matrix interfacial adhesion.

Recently, the obtainment of amorphous cellulose particles has been reported (Avolio et al., 2012). Due to their peculiar properties, i.e. the low crystallinity and aspect ratio, in this work amorphous cellulose particles have been tested for the first time as potential fillers for composites based on a biodegradable polyester, namely PCL. Medium and short length commercial cellulose fibers have been tested for comparison. Moreover, a compatibilization strategy already reported in a previous work (Haque, Errico, Gentile, Avella, & Pracella, 2012) has been applied to these systems to improve

* Corresponding author. Tel.: +39 081 8675057; fax: +39 081 8675230.
E-mail address: gennaro.gentile@ictp.cnr.it (G. Gentile).
[1] These authors equally contributed to the work.

http://dx.doi.org/10.1016/j.carbpol.2014.11.024
0144-8617/

Table 1
Main properties of commercial and amorphized cellulose.

Code	Description	Average length (μm)[a]	Average diameter (μm)[a]	Aspect ratio (l/d)	Crystallinity[b]
MLC	Medium length cellulose fibers	700	20	35	0.59
SLC	Short length cellulose fibers	200	20	10	0.53
AC	Amorphized cellulose	12	7.8	1.5	0.15

[a] Data from technical datasheets for MLC and SLC, and obtained for AC as described by Avolio et al. (2012).
[b] Values calculated for all the samples by WAXD analysis using the amorphous subtraction method (Avolio et al., 2012).

the polymer/filler interfacial adhesion. The obtained composites have been tested through physico-mechanical characterizations and soil burial degradation tests, in order to evaluate the influence of cellulose structure and morphology on the final properties of the realized materials.

2. Materials and methods

2.1. Materials

PCL CAPA 6506, molecular weight (MW) 50,000 g mol^{-1}, melt flow rate (MFR) 10 g (10 min)$^{-1}$ (at 160 °C/2.16 kg), was purchased from Solvay.

Medium length wood pulp cellulose fibers, trade name Arbocel BC1000, and short length wood pulp cellulose fibers, trade name Arbocel BWW40, were supplied by JRS Pharma GmbH (Rosenberg, Germany). Amorphized cellulose particles were obtained starting from Arbocel BWW40, as described in a previous work (Avolio et al., 2012), through a dry mechano-chemical treatment. Main characteristics of the cellulose fillers are summarized in Table 1.

Maleic anhydride (purity 99.8%) (MA) and glycidyl methacrylate (GMA) (purity 97%) were purchased from Sigma-Aldrich (Italy). All other chemicals used in this work were reagent grade and used without further purification.

2.2. Synthesis of PCL-g-MAGMA

PCL-g-MAGMA was prepared in the melt by using a Brabender Plasticorder internal mixer (Haque et al., 2012; Laurienzo, Malinconico, Mattia, & Romano, 2006). A mixture constituted by 36 g of PCL, 2 g of MA and 0.5 g of dibenzoyl peroxide (DBPO) was first fed into the mixer at 100 °C and then 2 g of GMA were added dropwise. The reaction was carried out at 100 °C for 20 min at 60 rpm. Modified PCL (coded as PCL-MAGMA) was kept in an oven at 60 °C for 12 h under vacuum to remove possible unreacted components.

2.3. Preparation of composites

The composites were prepared in a Brabender Plasticorder internal mixer at 120 °C and 60 rpm. First, PCL was fed into the mixing chamber and after 2 min the cellulose phase was added and kept under mixing for further 8 min. When PCL-MAGMA was used to improve the polymer filler interfacial adhesion, it was fed into the mixing chamber together with plain PCL. Neat PCL and a blend PCL/PCL-MAGMA 90/10 by wt were processed for comparison in the same conditions. Codes and composition of the prepared samples are listed in Table 2. After mixing, samples were pelletized and compression molded at 120 °C to obtain sheets (thickness about 1 mm) and films (thickness about 100 μm).

2.4. Analytical techniques

Morphological analysis of the realized materials was performed by using a scanning electron microscope (SEM) FEI Quanta 200 FEG on cryogenically fractured surfaces. SEM observations were performed in low vacuum mode ($P_{H_2O} = 0.7$ torr), using a large field detector (LFD) and an acceleration voltage of 5–20 kV.

Tensile tests were performed on dumb-bell specimens (4 mm^2 cross-section, 1 mm thickness, 25 mm gauge length) at room temperature and cross-head speed of 10 mm/min by using an Instron machine model 4505, according to the ASTM D638 test method. Young's modulus (E), stress at yield (σ_y) and elongation at break (ε) were calculated as average values over at least 10 analyzed samples. Before mechanical tests, samples were conditioned at 25 °C and 50% relative humidity (RH) for 48 h.

Thermal properties of neat PCL and composites were investigated by differential scanning calorimetry (DSC) using a Mettler DSC 30 calorimeter, Mettler-Toledo, Inc., equipped with a liquid-nitrogen accessory for fast cooling. The calorimeter was calibrated in temperature and energy using indium. Dry nitrogen was used as purge gas at a rate of 30 ml min^{-1}. DSC measurements were performed on small piece of compression-molded sample, weighting about 10 mg, encapsulated in a standard 40 μl aluminum pan. For DSC analyses samples were heated from −50 to 120 °C at a rate of 10 °C min^{-1}, held at 120 °C for 5 min to erase previous thermal history, cooled to −50 °C at 10 °C min^{-1}, then the samples were heated again at 10 °C min^{-1} until complete melting. For each sample the analysis was repeated tree times. Crystallization temperature (T_c) and onset crystallization ($T_{c_{onset}}$) temperature were recorded for each sample from the cooling run whereas melting temperature (T_m) and crystallinity (X_c) were recorded from the 2nd heating run. Crystallinity values of the composite samples were calculated considering the effective polymeric content. More specifically, X_c was calculated from the areas of the corresponding melting peaks according to the equation:

$$X_c = \frac{\Delta H}{w \Delta H^0} \times 100 \quad (1)$$

where w is the weight fraction of PCL + PCL-MAGMA in the composite and ΔH^0 is the specific heat of fusion of PCL in the fully crystalline state, 139.5 J g^{-1} (Crescenzi, Mancini, Calzolari, & Borri, 1972).

Table 2
Codes and composition of the prepared materials.

Codes	Composition (wt%)				
	PCL	PCL-MAGMA	MLC	SLC	AC
PCL	100	–	–	–	
PCL/AC 90/10	90	–	–	–	10
PCL/AC 80/20	80	–	–	–	20
PCL/AC 70/30	70	–	–	–	30
PCL/SLC 90/10	90	–	–	10	
PCL/SLC 80/20	80	–	–	20	
PCL/SLC 70/30	70	–	–	30	
PCL/MLC 90/10	90	–	10	–	
PCL/MLC 80/20	80	–	20	–	
PCL/MLC 70/30	70	–	30	–	
PCL/PCL-MAGMA	90	10	–	–	
C10-PCL/AC 80/20	72	8	–	–	20
C10-PCL/SLC 80/20	72	8	–	20	
C10-PCL/MLC 80/20	72	8	20	–	
C5-PCL/AC 80/20	76	4	–	–	20

For the isothermal crystallization analyses, samples were heated from 25 to 100 °C at 10 °C min^{-1}, held for 5 min at this temperature to ensure complete melting and to eliminate residual anisotropy. Subsequently, the samples were quickly cooled from 100 to the selected temperature (T_c = 38, 40 and 42 °C) at the rate of 30 °C min^{-1}. Samples were held at desired temperature to complete the crystallization process till no change in the heat flow was recorded.

Thermal degradation phenomena of PCL and PCL based composites were analyzed using a thermogravimetric analyzer (TGA) Perkin Elmer Pyris Diamond TG/DTA. A small piece (about 10 mg) of each sample was placed in a platinum open pan and heated from 50 to 600 °C at 10 °C min^{-1}. High purity nitrogen was fluxed through the furnace at a flow rate of 50 ml min^{-1}.

Water absorption tests were carried out in accordance to EN ISO 62:1999 (Dhakal, Zhang, & Richardson, 2007), by immersing the specimens in a deionised water bath at 25 °C. All the specimens were dried in a oven at 50 °C and then cooled to room temperature in a desiccator before weighing them to the nearest 0.1 mg. After immersion for different time, the specimens were taken out from the bath and the exceeding water was removed with a dry cotton textile. After that, the specimens were weighed to the nearest 0.1 mg and immersed again in the water bath. The specimens were weighed regularly after 15, 45, 120, 180, 300, 800 and 1500 min of immersion.

Water vapor transmission rate (WVTR) was measured according to the ASTM E96 standard, using the upright cup test. Film specimens, thickness about 100 μm, were conditioned for 48 h in a chamber at $T = 25 \pm 1$ °C and RH = 50 ± 1% before the test. Films were then sealed on cups containing distilled water and placed in the same conditioning environment. The permeation rate of the water vapor across the film was measured gravimetrically on three specimens for each sample, by weighting the cup every 24 h until the permeation rate reached a constant value.

Soil burial degradation tests were performed on film specimens, thickness about 100 μm, area about 7 cm^2. Films were buried in a local soil at the depth of 10 cm. Moisture content of soil was kept at around 50% by daily addition of water. The temperature recorded in the environment in the test period (April–June 2014) varied between 15 and 25 °C. The specimens were examined after 15, 45 and 75 days of soil burial by removing them carefully from the soil and washing them gently with distilled water. Weight loss due to biodegradation was evaluated on 3 specimens for each sample after drying them overnight at 40 °C under vacuum and conditioning at 25 °C and 50% RH for 24 h. Selected biodegraded specimens were also analyzed by SEM and TGA.

3. Results and discussion

In Table 1 main properties of cellulose samples used as fillers for the realization of PCL based composites are reported. As it can be observed, a significant reduction of the cellulose aspect ratio to a nearly circular shape (Avolio et al., 2012) is obtained as a consequence of the ball milling treatment, together with a very pronounced decrease of the crystallinity.

Due to these peculiar characteristics, in this work amorphized cellulose was tested as a possible filler for the realization of PCL based composites, in order to evaluate the effect of cellulose aspect ratio and crystallinity on the composite properties.

PCL composites were prepared by melt mixing with a cellulose content of 10, 20 and 30 wt%. Moreover, a compatibilization strategy based on the use of an interfacial agent obtained by reaction of PCL with maleic anhydride and glycidyl methacrylate (PCL-MAGMA) was applied to a selected number of systems, with the aim of evaluating the combined effect of the filler structure and the compatibilization on the final properties of the composites (Haque et al., 2012).

Codes and compositions of the prepared samples are reported in Table 2.

Tensile properties were recorded on the all sets of realized materials. All the other analytical techniques were applied on the complete set of samples containing amorphized cellulose (10, 20 and 30 wt% of AC content), to evaluate how this filler influenced the composite properties as a function of its relative amount. Instead, the effects induced either by the presence of amorphized cellulose with respect to short and medium length cellulose fibers, or by the use of the interfacial agent PCL-MAGMA was investigated at 20 wt% filler loading and at the maximum content of interfacial agent (PCL/PCl-MAGMA 90/10).

3.1. Morphological analysis

SEM micrographs of cryogenically fractured surfaces of uncompatibilized composite samples containing 20 wt% of cellulose filler are reported in Fig. 1. As it can be observed from the images at lower magnification, all the cellulose fillers are well distributed within the polymer matrix, independently of their average dimension and shape. Nevertheless, as a consequence of the mechanical stress applied during the cryogenic fracture, debonding and pull out phenomena of the fibers are well evident for both medium length and short length cellulose fibers (Fig. 1a–d), thus indicating a poor interfacial adhesion between the fibrous cellulose fillers and the polymer matrix. In the case of the composite sample containing amorphized cellulose (Fig. 1e–f), debonding phenomena are still evident, even if the lack of interactions between the phases seems to be reduced, the debonding of the filler from the matrix occurring leaving some polymer filaments linked to the amorphous cellulose phase.

On the contrary, as it can be observed from SEM micrographs reported in Fig. 2, in compatibilized samples all the cellulose fillers are well embedded within the polymer matrix, and an improved interfacial adhesion between the phases is evidenced. In particular, the composite failure occurs with a mechanism that clearly involves the fiber fracture more than the fiber pull out or the fiber matrix debonding. The improvement of PCL/cellulose interfacial adhesion in presence of the PCL-MAGMA compatibilizer can be attributed to the strong interactions occurring between hydroxyl groups of cellulose and anhydride groups of MA (Avella et al., 2007, 2008; Haque et al., 2012; Pracella, Chionna, Anguillesi, Kulinski, & Piorkowska, 2006).

In fact, as already reported (Laurienzo et al., 2006), the chemical modification of PCL with MA and GMA occurs without leaving a significant amount of unreacted epoxy groups, so that the possible chemical reaction between cellulose and residual epoxy groups should be considered negligible.

3.2. Tensile properties

In Table 3, tensile properties of the realized composites are reported.

As concerning uncompatibilized composites, for all the fillers tested, an increase of the elastic modulus was observed with respect to neat PCL as a function of the filler content. As expected, due to the high crystallinity and aspect ratio, this increase was more significant for composites containing 30 wt% of medium length cellulose fibers, about 280%, or short length cellulose fibers, about 240%. Reducing the aspect ratio of the filler led to a lower but still remarkable increase of the modulus. For materials containing 30 wt% of amorphized cellulose an increase of 185% was recorded.

By evaluating the stress at yield, it was found that for all the uncompatibilized systems, a progressive drop off of σ_y was

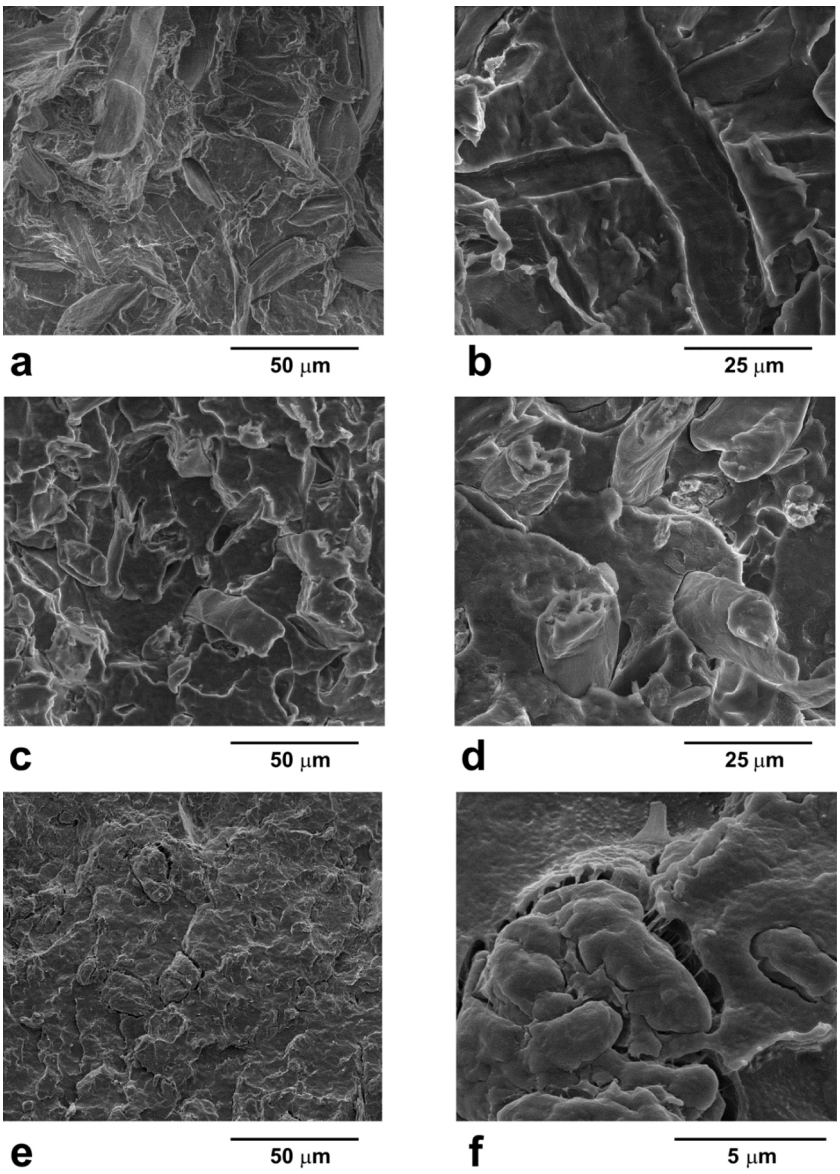

Fig. 1. SEM micrographs of uncompatibilized PCL based composites containing 20 wt% of cellulose fillers: (a–b) PCL/MLC 80/20; (c–d) PCL/SLC 80/20; (e–f) PCL/AC 80/20.

Table 3
Tensile properties of the realized composite samples.

Samples	E Young's modulus (MPa)	σ_y Stress at yield (MPa)	ε_b Elongation at break (%)
PCL	380 ± 11	16.5 ± 0.1	>1000%
PCL/AC 90/10	463 ± 6	13.9 ± 0.2	630 ± 42
PCL/AC 80/20	598 ± 11	12.5 ± 0.7	426 ± 21
PCL/AC 70/30	703 ± 12	10.5 ± 0.1	315 ± 29
PCL/SLC 90/10	489 ± 6	13.4 ± 0.1	546 ± 36
PCL/SLC 80/20	665 ± 32	11.5 ± 0.3	248 ± 79
PCL/SLC 70/30	917 ± 21	9.5 ± 0.5	15 ± 2
PCL/MLC 90/10	494 ± 9	13.2 ± 0.3	485 ± 48
PCL/MLC 80/20	714 ± 38	12.1 ± 0.5	18.6 ± 1.5
PCL/MLC 70/30	1063 ± 40	10.2 ± 0.4	2.5 ± 0.5
PCL/PCL-MAGMA	413 ± 13	17.8 ± 0.2	845 ± 75
C10-PCL/AC 80/20	629 ± 21	19.2 ± 0.3	21 ± 5
C10-PCL/SLC 80/20	738 ± 23	21.9 ± 0.3	13 ± 1
C10-PCL/MLC 80/20	742 ± 11	23.3 ± 0.5	11 ± 2
C5-PCL/AC 80/20	615 ± 17	17.1 ± 0.2	165 ± 35

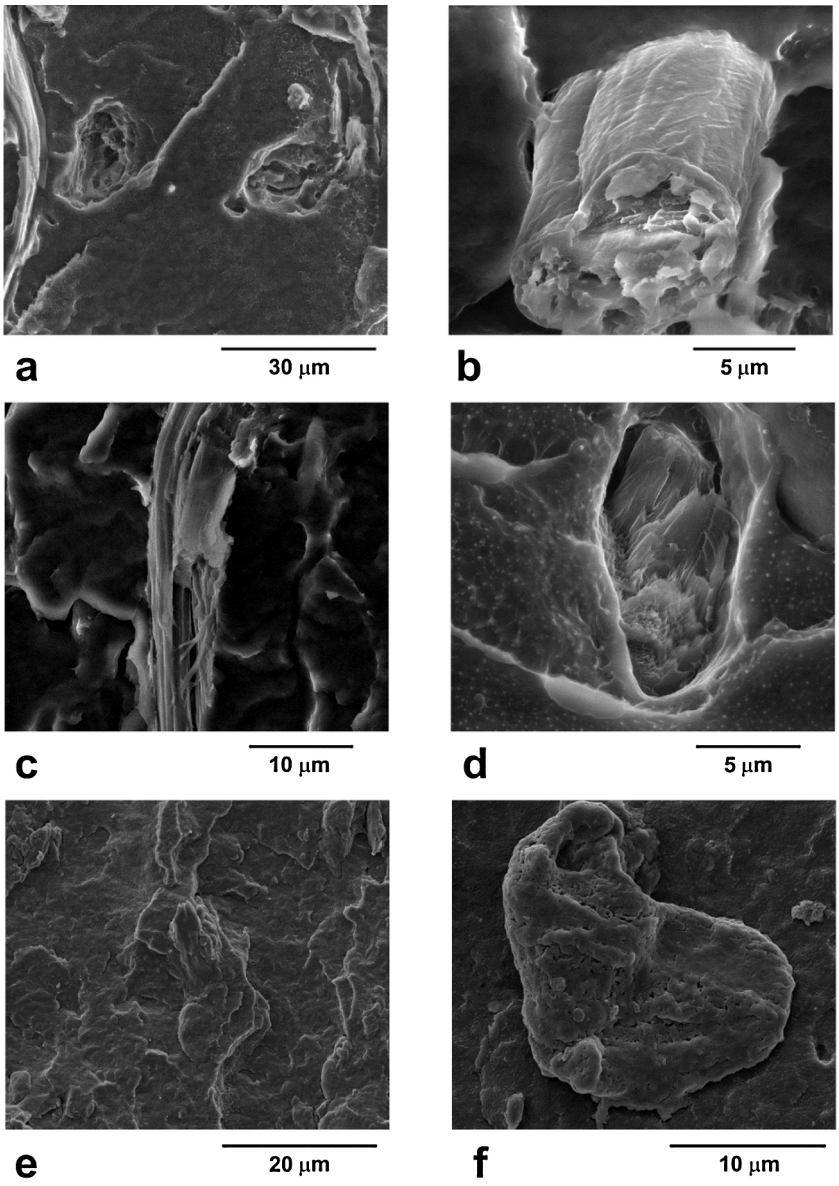

Fig. 2. SEM micrographs of compatibilized PCL based composites containing 20 wt% of cellulose fillers: (a–b) C10-PCL/MLC 80/20; (c–d) C10-PCL/SLC 80/20; (e–f) C10-PCL/AC 80/20.

recorded by increasing the amount of cellulose, irrespectively of the aspect ratio and crystallinity of the filler. In particular, the stress at yield decreased from 16.5 MPa for plain PCL to 9.5–10.5 MPa for composites filled with 30 wt% of medium length, short length cellulose fibers or amorphized cellulose particles.

Conversely, a significant effect of the cellulose aspect ratio and crystallinity of the filler was found on the elongation at break of the realized composites. For all the composites a significant reduction of this parameter was recorded with respect to neat PCL. Nevertheless, when medium length cellulose fibers were used as filler, the drop off of ε_b already occurred at 20 wt% filler loading (for PCL/MLC 80/20: $\varepsilon_b < 20\%$). By using short length fibers, at 20 wt% of fiber loading, the composite still kept a noticeable deformability, with $\varepsilon_b \sim 250\%$, and a significant decrease of ε_b occurred at 30 wt% of fiber loading (for PCL/SLC 70/30: $\varepsilon_b = 15\%$). On the contrary, in the case of amorphous cellulose, the ductile behavior of the material was preserved also at the highest content of filler, the sample PCL/AC 70/30 still showing a noticeable elongation at break, higher than 300%.

As concerning mechanical properties of compatibilized composites realized with a PCL/PCL-MAGMA 90/10 weight ratio, a significant increase of the stress at yield was obtained for all the systems. In particular, the increase was more relevant for the composite containing 20 wt% of medium cellulose fibers ($\sigma_y = 23.3$ MPa) and short length cellulose fibers ($\sigma_y = 21.9$ MPa). Nevertheless, also in the case of amorphized cellulose the stress at yield, 19.2 MPa, was higher than the corresponding value showed by the uncompatibilized composite or by neat PCL, thus confirming the effectiveness of the PCL-MAGMA to improve the polymer/cellulose interfacial adhesion.

As the effect of the adhesion is usually less relevant at low deformations, the influence of the coupling agent was found instead almost negligible on the elastic modulus of the composites.

However, the main drawback related to the use of PCL-MAGMA was the significant reduction of the elongation at break showed by all the compatibilized composites as a result of the polymer/filler interactions, responsible for a reduced macromolecular mobility that inhibits the ductile behavior of the material. Nevertheless, the

extent of this undesired drop off of ε_b was reduced by reducing the amount of interfacial agent (sample C5-PCL/AC 80/20, containing PCL/PCL-MAGMA in a weight ratio 95/5). This confirmed that by optimizing the amount of compatibilizer it was possible to balance the opposite effects of PCL-MAGMA, that is, the increase of yield stress and the reduction of ultimate strain.

3.2.1. Theoretical modeling of tensile modulus

The investigated set of PCL based materials, containing fillers with identical chemical composition but different aspect ratio, are particularly suitable to perform a comparison of the experimental tensile modulus with the predicted values obtained by theoretical models.

In particular, Halpin–Tsai equations represent a well known model to predict longitudinal and transverse moduli of aligned short fiber composites (Bhardwaj, Mohanty, Drzal, Pourboghrat, & Misra, 2006). The equations for the longitudinal (E_L) and transverse (E_T) moduli can be written as:

$$E_L = E_m \frac{1 + \xi \eta_L V_f}{1 + \eta_L V_f} \quad (2)$$

$$E_T = E_m \frac{1 + \xi \eta_T V_f}{1 + \eta_T V_f} \quad (3)$$

where:

$$\eta_L = \frac{\left(E_f/E_m\right) - 1}{\left(E_f/E_m\right) + \xi} \quad (4)$$

$$\eta_L = \frac{\left(E_f/E_m\right) - 1}{\left(E_f/E_m\right) + 2} \quad (5)$$

E_m and E_f are the elastic moduli of the matrix and fiber, respectively, V_f is the fiber volume fraction and ξ is a parameter depending on the shape of the filler. For fibrous reinforcements ξ can be approximated as $2l\,d^{-1}$, $l\,d^{-1}$ being the fiber aspect ratio.

For composites reinforced with fibers randomly oriented in a plane, the composite modulus E_{2D} can be predicted using the Tsai–Pagano equation (6) (Espinach et al., 2013):

$$E_{2D} = \frac{3}{8}E_L + \frac{5}{8}E_T \quad (6)$$

Nevertheless, deviations from 2D orientation induces a significant reduction of the composite stiffness. For a completely random orientation of the fibrous reinforcement in all three orthogonal directions, the composite modulus E_{3D} can be predicted using the following equation (Fornes & Paul, 2003):

$$E_{3D} = 0.184E_L + 0.816E_T \quad (7)$$

In Fig. 3, experimental tensile moduli of composite samples are compared with moduli values calculated by using Eq. (7) (solid lines). Filler volume fractions were calculated using density values of 1.145 (Izquierdo et al., 2008) and 1.5 (Facca, Kortschot, & Yan, 2006) $g\,cm^{-3}$ for neat PCL and cellulose reinforcements, respectively. For all the cellulose reinforcements, an average elastic modulus of 18 GPa was used in the calculations (Espinach et al., 2013; Zadorecki & Karnerfors, 1986) without taking into account different crystallinity values of the used cellulose materials.

As it can be observed, for all the tested reinforcements experimental data are in good agreement with theoretical values. No significant deviations were observed for composites containing amorphized cellulose, whereas higher deviations were observed with the increase of the average length of the cellulose reinforcement. In particular, passing from amorphized cellulose to SLC and MLC, also the differences between calculated and experimental values increased, with the model overestimating the modulus. The average deviation between experimental data points and model predictions was only 3% for the AC series, 8% for composites filled with SLC and about 20% for composites filled with MLC.

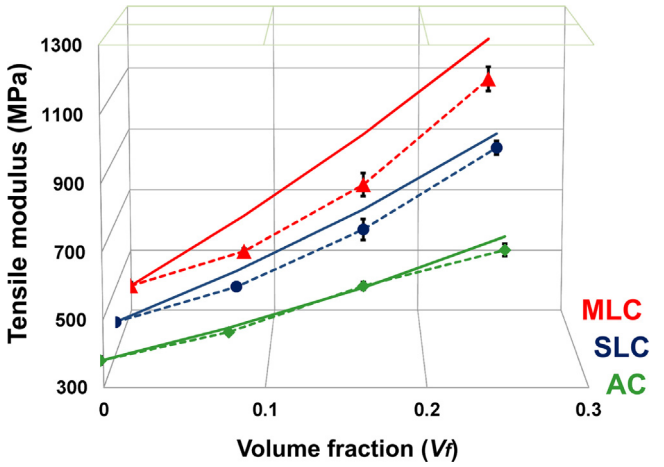

Fig. 3. Experimental tensile moduli of composite samples (dashed lines) compared with theoretical curves (solid lines) calculated by using Eq. (7).

This result was somewhat expected as the model used does not take into account the distribution of fiber length, which is usually wide for natural fibers. Moreover, longer fibers are more likely to be damaged and bent during the process thus reducing the effective aspect ratio in the composites.

3.3. Thermal and thermogravimetric analysis

3.3.1. Calorimetric analysis

DSC cooling and heating curves of PCL and composites containing different amount of amorphized, short and medium length cellulose are reported in Fig. 4. The crystallization temperature (T_c), the onset crystallization temperature ($T_{c_{onset}}$), the melting temperature (T_m) and the degree of crystallinity (X_c) calculated from DSC termograms for PCL and composites are listed in Table 4.

Crystallization of PCL occurs at 29.6, starting at about 34 °C and being complete at about 25 °C. As shown in Fig. 4a and in Table 4, the presence of the cellulose fillers induced an increase of the crystallization temperature, T_c, and the related onset temperature of PCL. In particular, T_c slightly shifted to higher temperature with increasing the amount of amorphized cellulose. As shown in Fig. 4c, a slight effect of the type of cellulose reinforcement on the crystallization temperature was also evidenced, although the numerical differences amongst T_c values shown by the composite samples are very small. As detailed below, the effect of cellulose shape and morphology has been thus investigated through isothermal crystallization analysis. Moreover, an increase of the crystallization

Table 4
Crystallization temperature (T_c) and onset ($T_{c_{onset}}$) temperature, melting temperature (T_m), and crystallinity degree (X_c).

Sample	T_c* (°C)	$T_{c_{onset}}$* (°C)	T_m* (°C)	X_c**
PCL	29.6	33.7	56.0	0.42
PCL/AC 90/10	33.0	35.7	56.0	0.43
PCL/AC 80/20	34.3	36.5	55.8	0.47
PCL/AC 70/30	35.0	36.9	55.8	0.48
PCL/SLC 80/20	34.5	37.2	55.9	0.43
PCL/MLC 80/20	34.9	37.7	55.9	0.40
PCL/PCL-MAGMA	33.5	36.9	55.5	0.58
C10-PCL/AC 80/20	34.8	37.1	55.9	0.50
C10-PCL/SLC 80/20	34.7	37.1	55.8	0.53
C10-PCL/MLC 80/20	34.8	37.3	55.8	0.50

Standard deviation values: * <1 °C; ** <0.03.

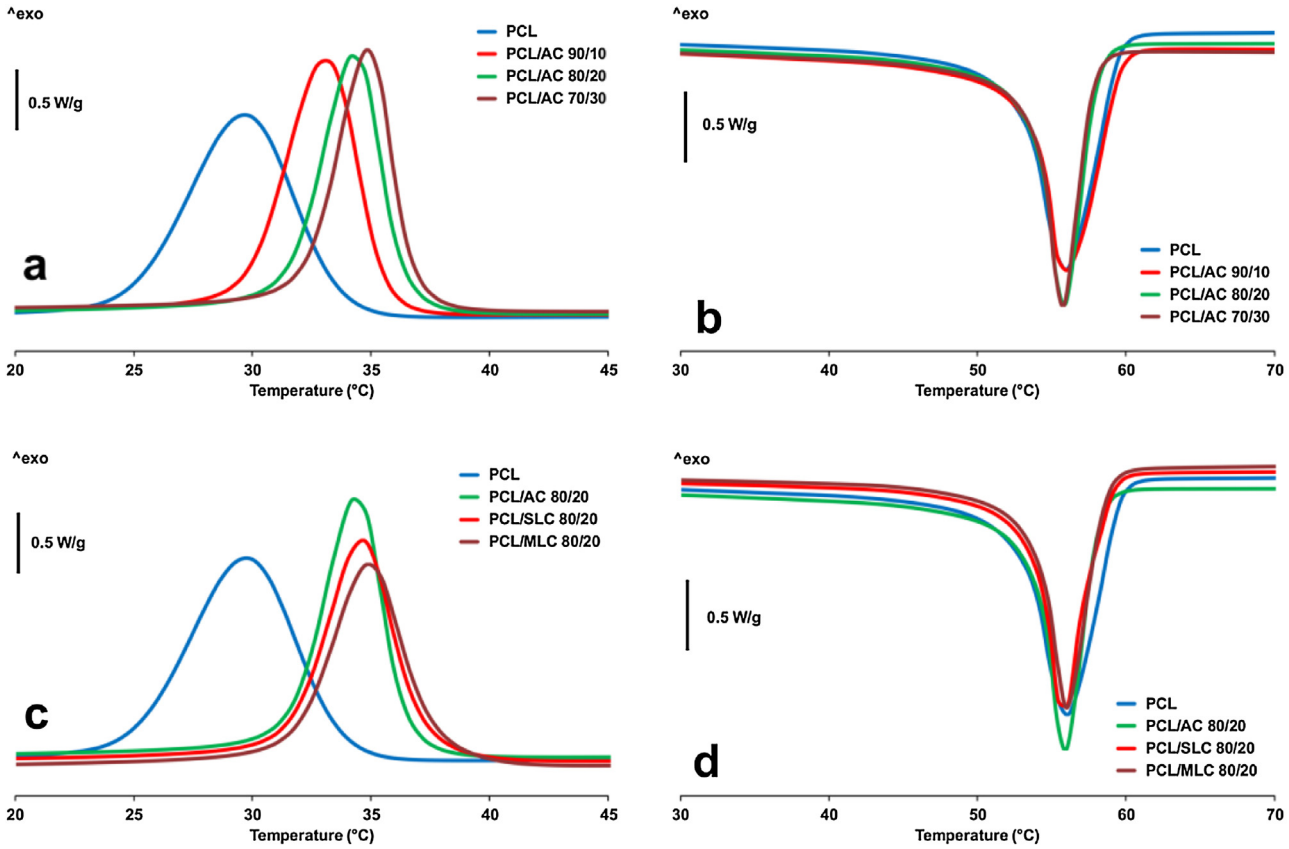

Fig. 4. DSC curves of PCL and PCL based composites: (a–b) cooling and 2nd heating run of PCL and PCL composites containing different amounts of amorphized cellulose; (c–d) cooling and 2nd heating run of PCL and PCL composites containing 20 wt% of MLC, SLC and AC.

temperature was also recorded for all the compatibilized composites with respect to neat PCL. This increase was comparable to that recorded for the corresponding uncompatibilized samples, thus indicating a negligible effect of the polymer/filler interfacial adhesion on the matrix crystallization.

As concerning the melting behavior, all the samples exhibited an endothermic peak corresponding to the melting of PCL phase. Nevertheless, as illustrated in Fig. 5b and c and already reported (Haque et al., 2012), the presence of the cellulose fillers did not significantly affect the melting temperature of the PCL matrix.

Moreover, even though all cellulose fillers act as nucleating agents, they are not able to increase the crystallinity of PCL. In fact, as presented in Table 4, all composites showed crystallinity values very close to that of neat PCL. An appreciable increase of X_c values with respect to neat PCL was found only for the compatibilized composites, but this effect can be mainly attributed to the presence of the interfacial agent PCL-MAGMA, this sample having higher crystallinity values with respect to PCL.

3.3.2. Isothermal crystallization analysis

In order to better elucidate possible differences on the crystallization process of PCL due to crystallinity and aspect ratio of the cellulose reinforcement, the crystallization behavior of PCL and composites was also investigated in isothermal conditions. The heat evolved during the crystallization of PCL and composites was then recorded as a function of time, and the fraction of material crystallized after a period of time t (X_t) was calculated from the ratio of the heat evolved at time t and the total heat evolved during the phase transformation, according to the following equation (Lorenzo, Arnal, Albuerne, & Muller, 2007):

$$X_t = \frac{\int_0^t \left(dH_c/dt\right) dt}{\int_0^\infty \left(dH_c/dt\right) dt} \quad (8)$$

The evolution at constant temperature of the degree of crystalline conversion, X_t, versus time for PCL and composites containing AC, SLC and MLC is reported in Fig. 5. Crystallization half-time ($\tau_{1/2}$), defined as the time needed to develop 50% of the final crystallinity, of PCL and composites are listed in Table 5.

As expected, in the analyzed range, for all the materials the phase transition rate decreases with T_c. As an example, this trend is shown in Fig. 5a for the PCL/AC 90/10 sample. Moreover, as it can be observed in Fig. 5b and c and from $\tau_{1/2}$ values reported in Table 5, the addition of cellulose reduced the crystallization half-time of PCL in the composites, thus indicating an increase in crystallization rate. This finding confirmed the non-isothermal DSC results, which have revealed that the addition of cellulose accelerates the crystallization of PCL.

By evaluating the results obtained for the PCL/AC series, see Fig. 5b, crystallization half-time were shortened by increasing the relative amount of amorphous cellulose. For instance, $\tau_{1/2}$ at 42 °C, whose value was 16.6 min for neat PCL, passed from 11.7 min for PCL/AC 90/10 to 8.6 min for PCL/AC 80/20 and to 8.2 min for PCL/AC 70/30. A similar behavior was recorded for all the investigated crystallization temperatures, thus confirming that the extent of the nucleating effect is a function of the cellulose content.

As concerning the effect of the different cellulose reinforcements used, evaluated at 20 wt% of filler content and illustrated in Fig. 5c, the increase of the fiber length and crystallinity induced an

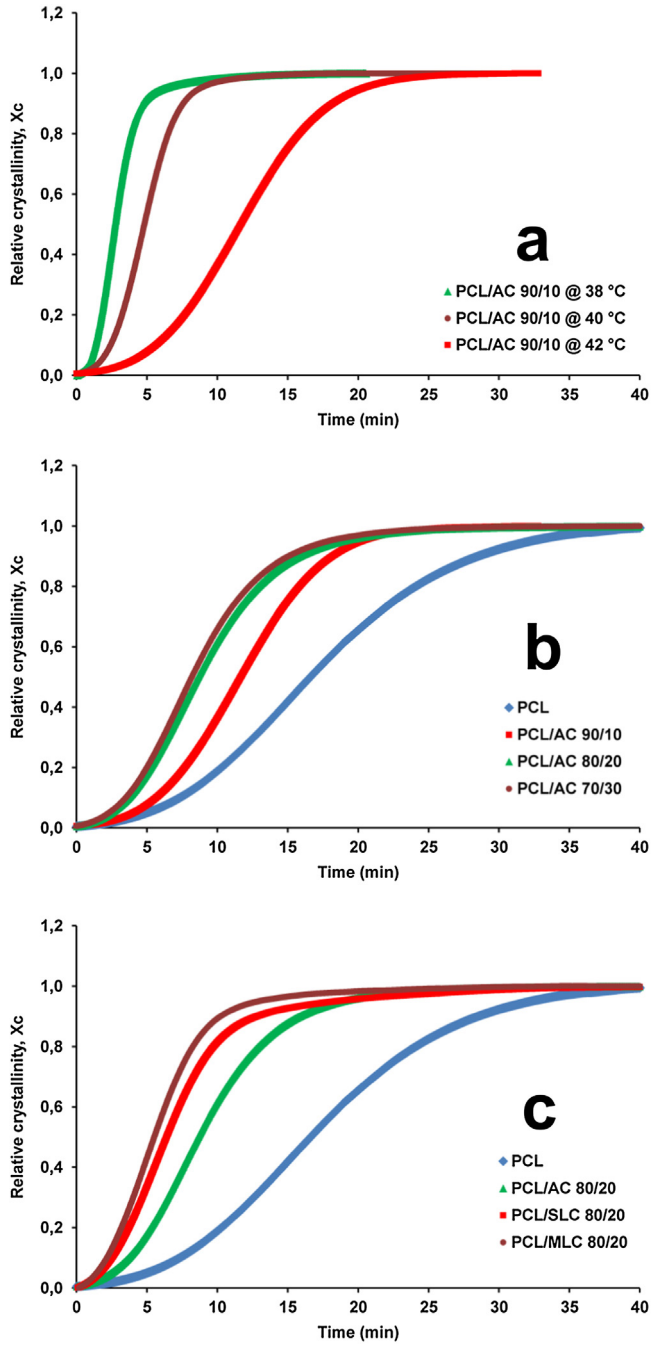

Fig. 5. Plots of X_t versus t for the isothermal crystallization of samples: (a) PCL/AC 90/10 at different crystallization temperatures; (b) isothermal crystallization at 42 °C of neat PCL, PCL/AC 90/10, PCL/AC 80/20 and PCL/AC 70/30; (c) isothermal crystallization at 42 °C of neat PCL, PCL/AC 80/20, PCL/SLC 80/20 and PCL/MLC 80/20.

appreciable progressive decrease of the crystallization half-time. This trend was evident at low crystallization rates. In particular, for the crystallization temperature of 42 °C, the crystallization half-time decreased from 16.6 min (neat PCL) to 8.6 min for PCL/AC 80/20, to 6.4 min for PCL/SLC 80/20 and to 5.2 min for PCL/MLC 80/20. Therefore, by the isothermal crystallization analysis, a progressive increase of the crystallization rate was evidenced passing from the composites containing longer and highly crystalline fibers (MLC) to the composite filled with intermediate fibers (SLC) and lastly with the amorphized cellulose (AC). This behavior indicated a less efficient nucleating effect of the amorphized cellulose particles with respect to the short and medium length cellulose fibers.

Table 5
Avrami kinetic parameters ($\tau_{1/2}$, K and n) and ΔE values for the isothermal crystallization of neat PCL and PCL based composites.

Sample	T_c (°C)	$\tau_{1/2}$ (min)	K (min^{-1})	n	ΔE (kJ mol^{-1})
PCL	38	3.3	0.0547	2.1	328.3
	40	8.2	0.0093	2.0	
	42	16.6	0.0010	2.3	
PCL/AC 90/10	38	2.7	0.0501	2.6	303.1
	40	4.8	0.0105	2.6	
	42	11.7	0.0010	2.6	
PCL/AC 80/20	38	1.9	0.1649	2.2	311.8
	40	3.4	0.0098	2.9	
	42	8.6	0.0045	2.3	
PCL/AC 70/30	38	1.6	0.2547	2.3	350.2
	40	3.2	0.0247	2.7	
	42	8.2	0.0062	2.2	
PCL/SLC 80/20	38	1.8	0.1735	2.0	247.9
	40	3.6	0.0502	2.0	
	42	6.4	0.0152	2.0	
PCL/MLC 80/20	38	1.9	0.1775	2.2	229.2
	40	3.1	0.0412	2.2	
	42	5.2	0.0219	2.0	
PCL/PCL-MAGMA	38	3.1	0.0661	2.0	294.3
	40	6.0	0.0081	2.5	
	42	12.9	0.0012	2.4	
C10-PCL/AC 80/20	38	1.5	0.3141	2.0	269.6
	40	2.8	0.0925	2.0	
	42	5.5	0.0104	2.4	
C10-PCL/SLC 80/20	38	1.5	0.2682	2.2	236.4
	40	2.5	0.1131	2.0	
	42	4.9	0.0175	2.3	
C10-PCL/MLC 80/20	38	2.3	0.1549	2.0	212.9
	40	2.8	0.0424	2.2	
	42	4.8	0.0192	2.0	

Moreover, a decrease of the $\tau_{1/2}$ values was observed for the compatibilized composites with respect to the corresponding uncompatibilized composites, but also in this case this effect can be explained considering the lower $\tau_{1/2}$ values shown by the interfacial agent PCL-MAGMA with respect to neat PCL.

Isothermal crystallization data were also analyzed using the Avrami equation (Lorenzo et al., 2007):

$$1 - X_t = \exp\left(Kt^n\right) \tag{9}$$

where X_t is the degree of crystalline conversion, K is the crystallization rate constant and n is the Avrami index, a parameter that provides a qualitative indication of the mechanisms of nucleation and crystal growth. Experimental data well fitted the Avrami equation for plain PCL and the composites at any crystallization temperature and the plots of $\ln[-\ln(1-X_t)]$ versus $\ln(t)$ were found linear ($R^2 > 0.985$) from almost the beginning of crystallization to approximately the peak time, that is the time at which the maximum of crystallization rate occurs. At longer times, i.e. at higher crystallization conversion, the Avrami equation fails due to spherulite impingement and the occurring of secondary crystallization processes (Siqueira et al., 2011).

Avrami constants K and n are summarized in Table 5, in which the total activation energy ΔE was also reported, derived from Arrhenius equation:

$$\frac{1}{n}\ln K = \ln K_0 - \frac{\Delta E}{RT_c} \tag{10}$$

Table 6
TGA results for neat PCL and PCL based composites: onset degradation temperature, evaluated at 5 wt% of weight loss ($T_{d(95\%)}$), temperatures of maximum degradation rate ($T_{max,i}$) and weight loss of the corresponding degradation steps (WL_i).

Samples	$T_{d(95\%)}$ (°C)	Step 1		Step 2	
		$T_{max,1}$ (°C)	WL_1 (wt%)	$T_{max,2}$ (°C)	WL_2 (wt%)
PCL	326.6		–	401.6	95.6
PCL/AC 90/10	321.1	355.4	9.1	404.5	85.5
PCL/AC 80/20	299.1	329.6	15.3	402.9	76.8
PCL/AC 70/30	282.8	325.7	23.8	406.3	68.3
PCL/SLC 80/20	312.0	351.6	15.3	399.9	78.75
PCL/MLC 80/20	315.6	361.6	17.7	396.3	81.5
PCL/PCL-MAGMA	333.1	–	–	402.6	96.8
C10-PCL/AC 80/20	301.0	338.8	16.7	396.5	76.4
C10-PCL/SLC 80/20	314.5	353.0	17.3	396.1	73.0
C10-PCL/MLC 80/20	323.8	347.0	15.3	396.8	76.4

where K_0 is a temperature-dependent pre-exponential factor and R the universal gas constant (Siqueira et al., 2011).

For almost all materials and crystallization conditions, n was found in the range between 2.0 and 2.6, revealing that polymeric chains in pure PCL and in the composites adopted a two-dimensional crystallization growth mechanism with a heterogeneous type of nucleation, in agreement with literature data (Liu et al., 2010).

Moreover, neat PCL showed an activation energy, ΔE, of 328 kJ mol^{-1}. This value slightly decreases to 303 kJ mol^{-1} when PCL was filled with 10 wt% of amorphised cellulose. However, at a higher AC content (20 and 30 wt%) the activation energy increased again to 312 and 350 kJ mol^{-1} due to the opposing effect of easier nucleation and hindered polymer chain transport. Consistently with the faster crystallization of PCL in the presence longer cellulose fibers, for composites containing 20 wt% of SLC and MLC the activation energy values were found lower (248 and 229 kJ mol^{-1}, respectively) with respect to the composite sample containing 20 wt% of amorphized cellulose, confirming the more efficient nucleating effect of the crystalline and fibrous reinforcement.

Finally, a progressive reduction of the activation energy values was found for the compatibilized composites with respect to the corresponding uncompatibilized composites. Nevertheless, the extent of the reduction of ΔE values for the compatibilized composites with respect to the system PCL-PCL-MAGMA was comparable to the decrease recorded for the corresponding uncompatibilized samples in comparison to neat PCL. This finding confirmed the negligible effect of the polymer/filler interfacial adhesion on the crystallization kinetics of the PCL matrix.

3.3.3. Thermogravimetric analysis

Thermal stability of neat PCL and composite samples was evaluated by means of thermogravimetric analysis. The temperature corresponding to a weight loss of 5 wt% ($T_{d(95\%)}$) as well as the temperatures corresponding to the maximum degradation rate are summarized in Table 6. Under nitrogen flow, neat PCL showed a broad degradation step whose onset, evaluated at 5 wt% of weight loss, was at $T_{deg(95\%)}$ = 327 °C and with a maximum degradation rate at T_{max} = 402 °C. As concerning the composite samples, all the composites showed a 2-step degradation mechanism. The first step showed a maximum degradation rate, $T_{max,1}$, between 345 and 362 °C. This step can be clearly attributed to the degradation of the cellulose fraction within the composite (Avolio et al., 2012). Considering the PCL/AC series, increasing the amount of cellulose from 10 to 30 wt%, the weight loss associated to this degradation step increased from 9.9 to 22 wt%. As concerning the second degradation step, whose maximum degradation rate was found ranging at temperatures $T_{max,2}$ between 395 and 405 °C, it was attributed to the degradation of the PCL phase. Furthermore, thermogravimetric analysis of composite samples realized with SLC and MLC did not show significant differences with respect to the corresponding composites containing amorphized cellulose. No significant differences were recorded also for compatibilized composite samples, thus confirming that either the use of the amorphized cellulose filler, either the proposed interfacial strategy did not affect the thermal stability of the composites.

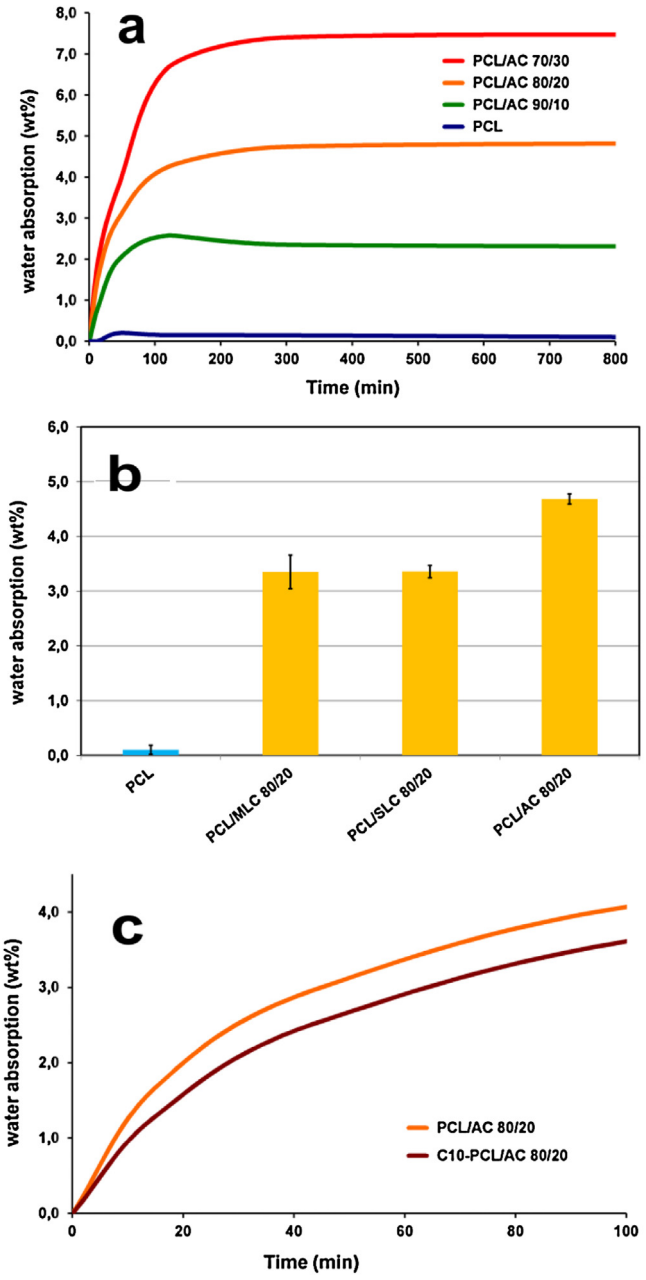

Fig. 6. Results of water absorption tests: (a) typical water absorption curves of neat PCL and PCL based composites containing amorphized cellulose; (b) comparison of equilibrium water absorption values for PCL and PCL based composites containing 20 wt% of various cellulose fillers; (c) first part of a typical water absorption curve for the plain and the compatibilized composite containing 20 wt% of amorphized cellulose.

3.4. Water absorption and water vapor permeability

Water absorption tests were carried out in order to evaluate how the hydrophilicity of cellulose can influence the absorption

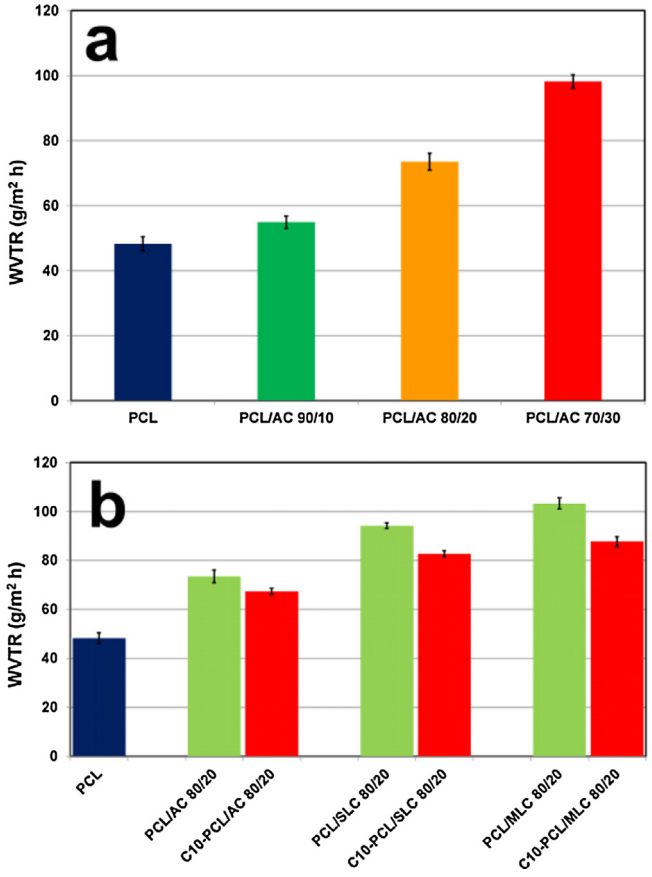

Fig. 7. Results of WVTR tests: (a) WVTR of neat PCL and PCL based composites containing amorphized cellulose; (b) WVTR of PCL and plain and compatibilized PCL based composites containing 20 wt% of various cellulose fillers.

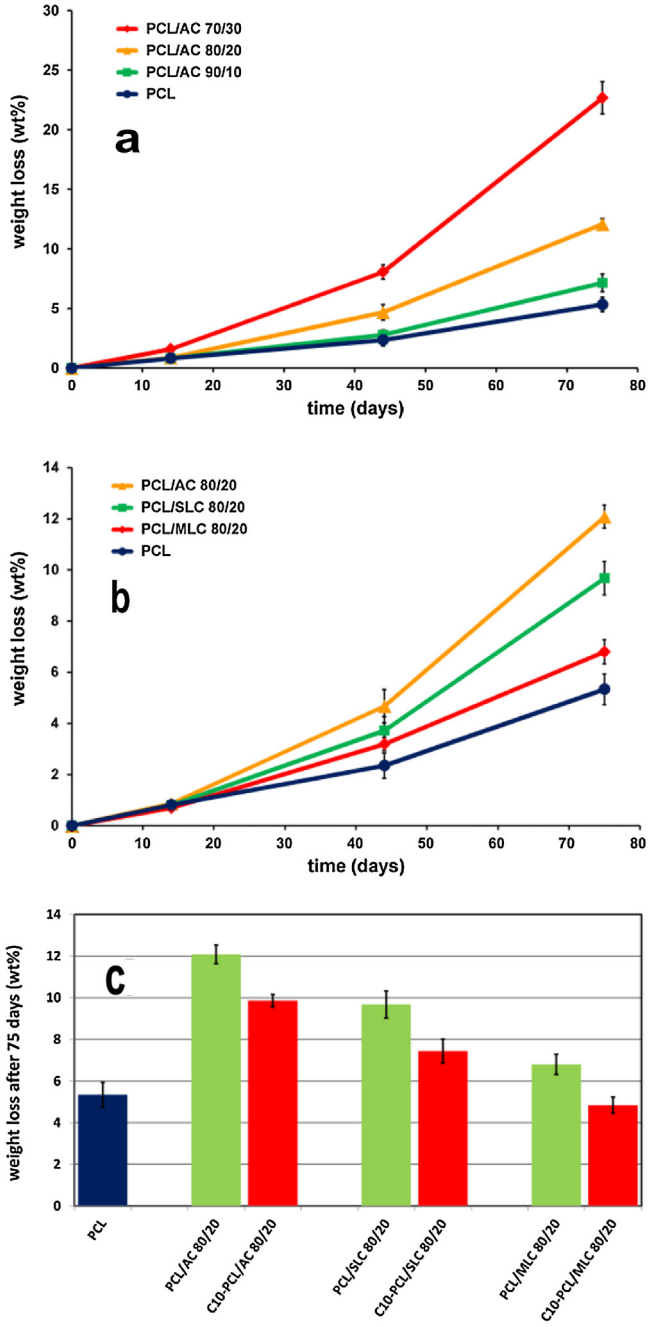

Fig. 8. Results of the soil burial degradation tests of PCL and PCL based composites: (a) weight loss vs. time of PCL and composites containing different amounts of AC; (b) weight loss vs. time of PCL and composites containing 20 wt% of MLC, SLC and AC; (c) weight loss after 75 days of soil burial degradation pf compatibilized and uncompatibilized composites containing 20 wt% of MLC, SLC and AC.

behavior of PCL based composites, a property that can affect both the mechanical properties of the materials in high relative humidity environments (Avella, Cocca, Errico, & Gentile, 2012; Sgriccia, Hawley, & Misra, 2008) and the rate of the biodegradation (Ismail & Zaaba, 2012), thus determining the possible application sectors.

Typical water absorption curves of PCL/AC composites are reported in Fig. 6a. As it can be observed, progressively increasing the content of the hydrophilic filler, a significant increase of the water absorption is recorded. Neat PCL shows a water uptake of about 0.1 wt%, whereas PCL/AC containing 10, 20 and 30 wt% of amorphized cellulose show equilibrium water absorption values of 2.4, 4.7 and 7.4 wt%, respectively.

In Fig. 6b, the effect of the type of cellulose filler used for the realization of the composites is illustrated. For PCL based composites containing 20 wt% of cellulose, MLC and SLC induce a comparable water absorption of the composites, between 3.7 and 3.9 wt%, whereas when the amorphized filler is used, an increase of the water absorption is recorded, up to 4.7 wt%. This effect is clearly attributed to the presence of the amorphous cellulose phase that has been already proven to absorb higher amount of water, because the amorphous fraction is more accessible to water molecules with respect to the cellulose crystalline domains (Avolio et al., 2012).

As concerning the effect of the interfacial adhesion between the phases, no significant changes in the equilibrium water absorption were recorded after 800 min of test for the compatibilized composites with respect to the uncompatibilized ones. However, a slight decrease of the water absorption rate was observed for the compatibilized composites in the first part of the water absorption curve, as it can be observed in Fig. 6c. The effect is similar for the composites containing 20 wt% of MLC and SLC, thus indicating that an improved polymer filler interfacial adhesion can effectively decrease the water absorption rate.

Water vapor permeability properties of cellulose filled composites are particularly relevant, especially for typical PCL applications, like packaging. In fact, owing to high hydrophilic nature of the reinforcement, most of these materials show poor barriers to water vapor. Nevertheless, apart from its own hydrophilicity, the filler can influence barrier properties also depending on its dispersion and distribution within the polymer matrix (Khan et al., 2013; Lagaron, Catala, & Gavara, 2004).

WVTR values recorded for neat PCL and composites are illustrated in Fig. 7. The reported numerical values, in $g\,m^{-2}\,h^{-1}$, are

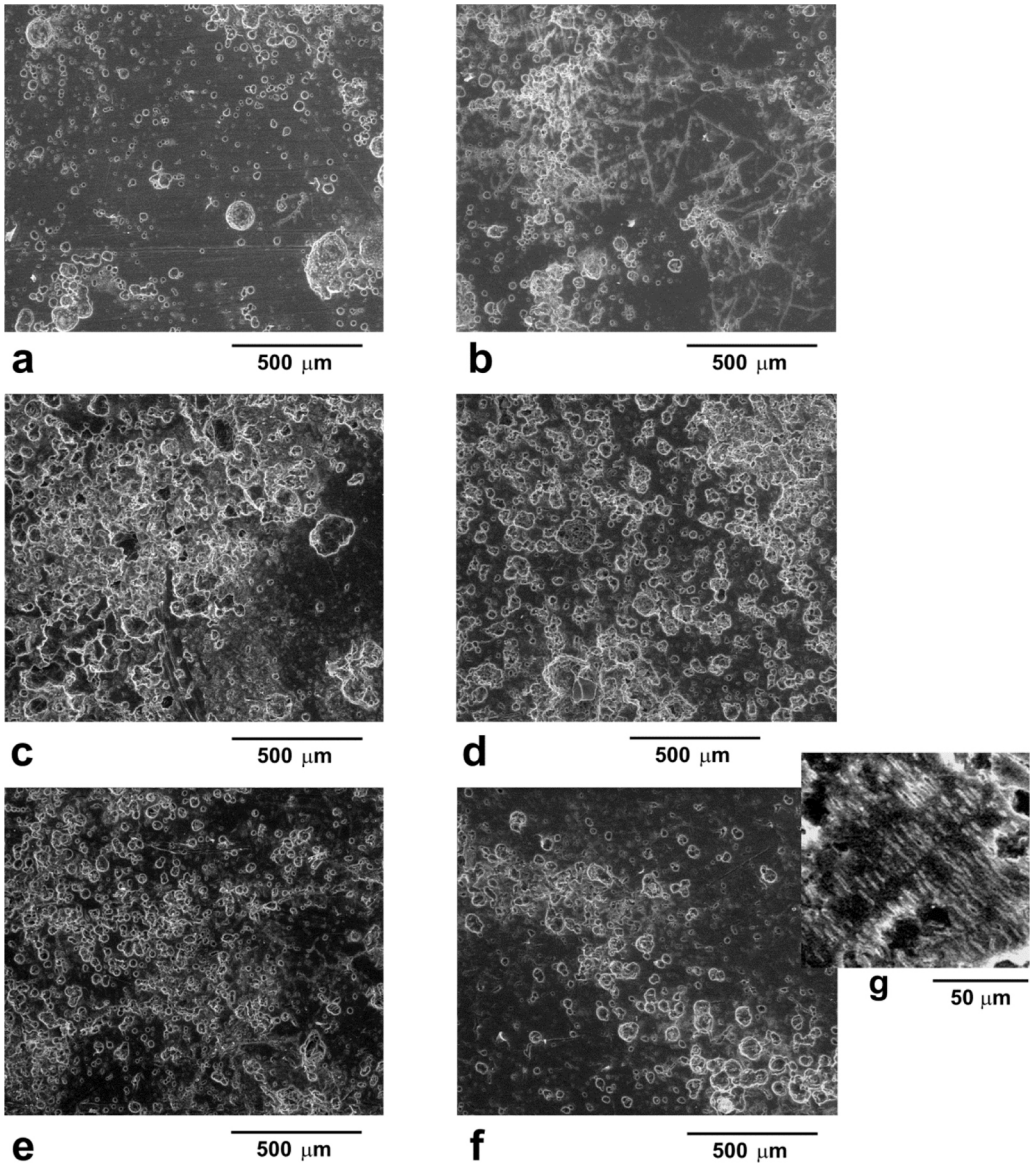

Fig. 9. SEM micrographs of the outer surface of neat PCL and PCL based composites after 75 days of soil burial degradation: (a) PCL; (b) PCL/AC 90/10; (c) PCL/AC 80/20; (d) PCL/AC 70/30; (e) PCL/SLC 80/20; (f–g) PCL/MLC 80/20.

normalized to a film thickness of 100 μm using the equation (Shogren, 1997):

$$\mathrm{WVTR} = \frac{\mathrm{WVTR}_{(\mathrm{raw})} \times t}{100} \quad (10)$$

where t is the measured thickness of the films in μm.

As it can be observed from Fig. 7a, progressively increasing the content of the hydrophilic filler, a progressive increase of WVTR is recorded. In particular, neat PCL shows a WVTR of $48.3 \pm 2.2\,\mathrm{g\,m^{-2}\,h^{-1}}$. This value is consistent to literature data (Shogren, 1997). Increasing the AC content within the composites, WVTR values increase to $54.9 \pm 1.9\,\mathrm{g\,m^{-2}\,h^{-1}}$ (at 10 wt% AC content), to $73.5 \pm 2.6\,\mathrm{g\,m^{-2}\,h^{-1}}$ (at 20 wt% AC content), and to $98.2 \pm 2.1\,\mathrm{g\,m^{-2}\,h^{-1}}$ (at 30 wt% AC content). This trend is similar to what already reported for the water absorption tests and it is clearly dependent on the hydrophilic nature of the filler.

Nevertheless, by observing Fig. 7b, it is possible to note that the WVTR for composites containing 20 wt% of AC, SLC or MLC follows a trend opposite to what observed for the equilibrium water absorption. Passing from the amorphized and more hydrophilic cellulose (AC) to the fibrous cellulose (SLC and MLC) a progressive increase of the WVTR is recorded. This behavior can be attributed to two different factors: the slight decrease of the crystallinity recorded for composites containing longer and more crystalline cellulose fillers, and the better dispersion of the particle-shaped amorphized cellulose with respect to the fibrous reinforcement. The presence of long fibers and a weak polymer/fibers interfacial adhesion create within the composite a sort of preferential path for water vapor molecules, thus increasing the permeation rate. This effect is progressively reduced by decreasing the fiber length.

Finally, as concerning the effect of the compatibilization, it can be observed that all the compatibilized composites show lower WVTR values with respect to the corresponding uncompatibilized ones. The extent of the recorded decrease ranges between 8%, for C10-PCL/AC 80/20, and about 15% for C10-PCL/MLC 80/20. As already reported for cellulose-filled composites containing an effective compatibilizing agent (Avella et al., 2009), this result can be explained taking into account that in compatibilized composites fibers are well wetted by the polymer phase that can protect them from the water diffusion. Moreover, also in this case the increased

crystallinity recorded for the compatibilized composites can contribute to the decrease of the permeation rate.

3.5. Biodegradation tests

Soil burial degradation tests were carried out to evaluate the effect of the crystal structure and morphology of the cellulose filler on the biodegradation kinetic of the composites. The results, expressed as weight loss vs. time, are illustrated in Fig. 8.

In particular, in Fig. 8a the results obtained for composites containing different amounts of amorphized cellulose are reported in comparison to neat PCL. As it can be observed, increasing the content of amorphized cellulose, a progressive increase of the degradation rate is recorded. As concerning the effect of the cellulose crystallinity and morphology, illustrated in Fig. 8b, it can be observed that composites containing amorphized cellulose undergo a faster degradation with respect to composites containing short and medium length cellulose fibers. Finally, as shown in Fig. 8c, the degradation kinetic recorded for compatibilized composites is in all cases slowed down with respect to the corresponding uncompatibilized composites.

This behavior can be well explained taking into account the results of the water absorption test that have demonstrated the high water absorption capacity of the composites containing larger amounts of amorphized cellulose and the decrease of the water absorption rate for compatibilized composites.

Therefore it seems evident that the water intake plays a crucial role to determine the degradation kinetics of the composites. The presence of amorphized cellulose, able to absorb higher amounts of water, induces an appreciable increase of the biodegradation kinetic and this effect is more evident at high filler loadings. On the contrary, a lower water sorption capacity of the materials, due for instance to the presence of short or medium length cellulose fibers or, even more, to an improved polymer/filler interfacial adhesion in the case compatibilized composites, induces a decrease of the soil burial degradation rate (Alvarez, Ruseckaite, & Vazquez, 2006).

SEM micrographs of the outer surface of neat PCL and selected composites after 75 days of soil burial degradation are reported in Fig. 9.

Neat PCL and all the composites underwent degradation through the formation of irregular holes on the sample surface. Moreover, in all the composites degraded for 75 days, a cellulose fraction was still observed at the morphological analysis. The presence of this fraction was confirmed and quantified by TGA analysis of the samples after 75 days of soil burial degradation tests, showing that the composition of the degraded samples, evaluated through the WL_1/WL_2 ratio (see also Table 6), remained almost unchanged and thus that the biodegradation process for all the composites involved both the cellulose and the PCL phases. Finally, the presence of grooves on the surface of the films, illustrated in Fig. 9g, was observed for all the composites. These grooves, attributed in literature to the degradation of the amorphous fraction of PCL (Hakkarainen & Albertsson, 2002), indicated that the degradation of the materials started not only from the cellulose fraction but also from the non-crystalline PCL phase.

4. Conclusions

Through the combined approach based on the use of amorphous cellulose particles and a suitable interfacial agent it was possible to modulate relevant technological properties of PCL based composites, such as tensile and thermal properties, water absorption and water vapor transmission rate and biodegradation kinetics.

Morphological analysis of cryogenically fractured composite surfaces revealed that the cellulose fillers are well distributed within the PCL matrix, independently of their average dimension and shape. Nevertheless, debonding and pull out phenomena of the fibers indicated a poor interfacial adhesion between cellulose and the polymer matrix. For all the systems the use of the modified PCL as interfacial agent was able to significantly improve the PCL/cellulose interfacial adhesion. Tensile tests carried out on the composite samples confirmed this behavior. Compatibilization was able to induce a significant improvement of the stress at yield for all the realized materials.

As concerning the elastic modulus, amorphous cellulose particles induced a less significant but still remarkable increase of the tensile modulus with respect to longer and more crystalline cellulose reinforcements.

Moreover, a significant effect of the cellulose aspect ratio and crystallinity of the filler was found on the elongation at break of the realized composites. For all the composites a significant reduction of this parameter was recorded with respect to neat PCL. Nevertheless, when medium length cellulose fibers were used as filler, the drop off of the elongation at break already occurred at 20 wt% filler loading, whereas in the case of amorphous cellulose, the ductile behavior of the material was preserved also at the highest content of filler, the sample containing 30 wt% of amorphous cellulose still showing a noticeable elongation at break, higher than 300%.

Non-isothermal and isothermal calorimetric analysis revealed a nucleating effect of all the cellulose fillers. Moreover, by the isothermal crystallization analysis, a less efficient nucleating effect of the amorphized cellulose particles with respect to longer and more crystalline cellulose fibers was evidenced.

As concerning the water absorption behavior, the use of the amorphized cellulose filler induced an appreciable increase of the water uptake, well explained because the amorphous fraction of cellulose is more accessible to water molecules with respect to the cellulose crystalline domains. A decrease of the water absorption rate was instead recorded for compatibilized composites. Furthermore, all the composite samples showed water vapor transmission rates higher than neat PCL. Nevertheless, the addition of amorphous cellulose particles to PCL induced a less significant increase of the water vapor permeability with respect to composites realized with longer and highly crystalline cellulose fibers. This trend was confirmed in presence of the interfacial agent.

Finally, soil burial degradation tests revealed that composites containing amorphized cellulose undergo a faster degradation with respect to composites containing short and medium length cellulose fibers. The biodegradation kinetic was slowed down for compatibilized composites. This behavior was explained taking into account the high water absorption capacity of the composites containing larger amounts of amorphized cellulose and the decrease of the water absorption rate recorded for compatibilized composites.

References

Alvarez, V. A., Ruseckaite, R. A., & Vazquez, A. (2006). Degradation of sisal fibre/Mater Bi–Y biocomposites buried in soil. *Polymer Degradation and Stability*, *91*, 3156–3162.

Avella, M., Bogoeva-Gaceva, G., Buzarovska, A., Errico, M. E., Gentile, G., & Grozdanov, A. (2007). Poly(3-hydroxybutyrate-*co*-3-hydroxyvalerate)-based biocomposites reinforced with kenaf fibers. *Journal of Applied Polymer Science*, *104*, 3192–3200.

Avella, M., Bogoeva-Gaceva, G., Buzarovska, A., Errico, M. E., Gentile, G., & Grozdanov, A. (2008). Poly(lactic acid)-based biocomposites reinforced with kenaf fibers. *Journal of Applied Polymer Science*, *108*, 3542–3551.

Avella, M., Avolio, R., Bonadies, I., Carfagna, C., Errico, M. E., & Gentile, G. (2009). Recycled multilayer cartons as cellulose source in HDPE-based composites: Compatibilization and structure–properties relationships. *Journal of Applied Polymer Science*, *114*, 2978–2985.

Avella, M., Cocca, M., Errico, M. E., & Gentile, G. (2012). Polyvinyl alcohol biodegradable foams containing cellulose fibres. *Journal of Cellular Plastics*, *48*, 459–470.

Avolio, R., Bonadies, I., Capitani, D., Errico, M. E., Gentile, G., & Avella, M. (2012). A multitechnique approach to assess the effect of ball milling on cellulose. *Carbohydrate Polymers*, *87*, 265–273.

Bastioli, C. (1998). Properties and applications of Mater-Bi starch-based materials. *Polymer Degradation and Stability*, *1–3*, 263–272.

Bhardwaj, R., Mohanty, A. K., Drzal, L. T., Pourboghrat, F., & Misra, M. (2006). Renewable resource-based green composites from recycled cellulose fiber and poly(3-hydroxybutyrate-*co*-3-hydroxyvalerate) bioplastic. *Biomacromolecules*, *7*, 2044–2051.

Bogoeva-Gaceva, G., Avella, M., Malinconico, M., Buzarovska, A., Grozdanov, A., Gentile, G., et al. (2007). Natural fiber eco-composites. *Polymer Composites*, *28*, 98–107.

Buzarovska, A., Bogoeva-Gaceva, G., Grozdanov, A., Avella, M., Gentile, G., & Errico, M. E. (2007). Crystallization behavior of poly(hydroxybytyrate-*co*-valerate) in model and bulk PHBV/kenaf fiber composites. *Journal Material Science*, *42*, 6501–6509.

Crescenzi, V., Mancini, G., Calzolari, G., & Borri, C. (1972). Thermodynamics of fusion of poly-β-propiolactone and poly-ε-caprolactone. Comparative analysis of the melting of aliphatic polylactone and polyester chains. *European Polymer Journal*, *8*, 449–463.

Cyras, V. P., Iannace, S., Kenny, J. M., & Vasquez, A. (2001). Relationship between processing and properties of biodegradable composites based on PCL/starch matrix and sisal fibers. *Polymer Composites*, *22*, 104–110.

Dányádi, L., Janecska, T., Szabó, Z., Nagy, G., Móczó, J., & Pukánszky, B. (2007). Wood flour filled PP composites: Compatibilization and adhesion. *Composites Science and Technology*, *67*, 2838–2846.

Dhakal, H. N., Zhang, Z. Y., & Richardson, M. O. W. (2007). Effect of water absorption on the mechanical properties of hemp fibre reinforced unsaturated polyester composites. *Composites Science and Technology*, *67*, 1674–1683.

Dimzoski, B., Bogoeva Gaceva, G., Gentile, G., Avella, M., Errico, M. E., & Srebrenkoska, V. (2008). Preparation and characterization of poly(lactic acid)/rice hulls based biodegradable composites. *Journal of Polymer Engineering*, *28*, 369–384.

Dominkovics, Z., Dányádi, L., & Pukánszky, B. (2007). Surface modification of wood flour and its effect on the properties of PP/wood composites. *Composites, A: Applied Science and Manufacturing*, *38*, 1893–1901.

Espinach, F. X., Julian, F., Verdaguer, N., Torres Ll Pelach, M. A., Vilaseca, F., & Mutje, P. (2013). Analysis of tensile and flexural modulus in hemp strands/polypropylene composites. *Composites, B: Engineering*, *47*, 339–343.

European Commission. (2013). *Green paper on a European strategy on plastic waste in the environment*. Brussels, Belgium: European Commission (COM(2013); 7.3.2013), ⟨http://ec.europa.eu/environment/waste/pdf/green_paper/green_paper_en.pdf⟩ (access August 2014).

Facca, A. G., Kortschot, M. T., & Yan, N. (2006). Predicting the elastic modulus of natural fibre reinforced thermoplastics. *Composites, A: Applied Science and Manufacturing*, *37*, 1660–1671.

Faludi, G., Dora, G., Renner, K., Móczó, J., & Pukánszky, B. (2013). Biocomposite from polylactic acid and lignocellulosic fibers: Structure–property correlations. *Carbohydrate Polymers*, *92*, 1767–1775.

Faruk, O., Bledzki, A. K., Fink, H.-P., & Sain, M. (2012). Biocomposites reinforced with natural fibers: 2000–2010. *Progress in Polymer Science*, *37*, 1552–1596.

Fornes, T. D., & Paul, D. R. (2003). Modeling properties of nylon 6/clay nanocomposites using composite theories. *Polymer*, *44*, 4993–5013.

Ganster, J., & Fink, H. P. (2006). Novel cellulose fibre reinforced thermoplastic materials. *Cellulose*, *13*, 271–280.

Hakkarainen, M., & Albertsson, A.-C. (2002). Heterogeneous biodegradation of polycaprolactone-low molecular weight products and surface changes. *Macromolecular Chemistry and Physics*, *203*, 1357–1363.

Haque, M.-U., Errico, M. E., Gentile, G., Avella, M., & Pracella, M. (2012). Functionalization and compatibilization of poly(ε-caprolactone) composites with cellulose microfibres: Morphology, thermal and mechanical properties. *Macromolecular Materials and Engineering*, *297*, 985–993.

Ismail, H., & Zaaba, N. F. (2012). Tensile properties degradation behavior, and water absorption of sago starch plastic films. *Journal of Vinyl and Additive Technology 2012*, *18*, 235–240.

Izquierdo, R., Garcia-Giralt, N., Rodriguez, T., Cáceres, E., García, S. J., Gómez Ribelles, J. L., et al. (2008). Biodegradable PCL scaffolds with an interconnected spherical pore network for tissue engineering. *Journal of Biomedical Materials Research, A 2008*, *85A*, 25–35.

John, M. J., & Thomas, S. (2008). Biofibres and biocomposites. *Carbohydrate Polymers 2008*, *71*, 343–364.

Joseph, K., & Thomas, S. (1996). Effect of chemical treatment on the tensile properties of short sisal fibre-reinforced polyethylene composites. *Polymer*, *37*, 5139–5149.

Keller, A. (2003). Compounding and mechanical properties of biodegradable hemp fibre composites. *Composites Science and Technology*, *63*, 1307–1316.

Khan, R. A., Beck, S., Dussault, D., Salmieri, S., Bouchard, J., & Lacroix, M. (2013). Mechanical and barrier properties of nanocrystalline cellulose reinforced poly(caprolactone) composites: Effect of gamma radiation. *Journal of Applied Polymer Science*, *129*, 3038–3046.

Lagaron, J. M., Catala, R., & Gavara, R. (2004). Overview: Structural characteristics defining high barrier properties in polymeric materials. *Material Science and Technology*, *20*, 1–7.

Laurienzo, P., Malinconico, M., Mattia, G., & Romano, G. (2006). Synthesis and characterization of functionalized crosslinkable poly(ε-caprolactone). *Macromolecular Chemistry and Physics*, *207*, 1861–1869.

Liu, H., Xie, F., Yu, L., Chen, L., & Li, L. (2009). Thermal processing of starch-based polymers. *Progress in Polymer Science*, *34*, 1348–1368.

Liu, H., Huang, Y., Yuan, L., He, P., Cai, Z., Shen, Y., et al. (2010). Isothermal crystallization kinetics of modified bamboo cellulose/PCL composites. *Carbohydrate Polymers*, *79*, 513–519.

Lorenzo, A. T., Arnal, M. L., Albuerne, J., & Muller, A. J. (2007). DSC isothermal polymer crystallization kinetics measurements and the use of the Avrami equation to fit the data: Guidelines to avoid common problems. *Polymer Testing*, *26*, 222–231.

Lu, D. R., Xiao, C. M., & Xu, S. J. (2009). Starch-based completely biodegradable polymer materials. *eXPRESS Polymer Letters*, *3*, 366–375.

Nampoothiri, K. M., Nair, N. R., & John, R. P. (2010). An overview of the recent developments in polylactide (PLA) research. *Bioresource Technology*, *101*, 8493–8501.

Nestore, O., Kajaks, J., Vancovicha, I., & Reihmane, S. (2013). Physical and mechanical properties of composites based on a linear low-density polyethylene (LLDPE) and natural fiber wastes. *Mechanics of Composite Materials*, *48*, 619–628.

Pracella, M., Chionna, D., Anguillesi, I., Kulinski, Z., & Piorkowska, E. (2006). Functionalization, compatibilization and properties of polypropylene composites with Hemp fibres. *Composites Science and Technology*, *66*, 2218–2230.

Siqueira, G., Fraschini, C., Bras, J., Dufresne, A., Prud'homme, R., & Laborie, M.-P. (2011). Impact of the nature and shape of cellulosic nanoparticles on the isothermal crystallization kinetics of poly(ε-caprolactone). *European Polymer Journal*, *47*, 2216–2227.

Siracusa, V., Rocculi, P., Romani, S., & Dalla Rosa, M. (2008). Biodegradable polymers for food packaging: A review. *Trends in Food Science & Technology*, *19*, 634–643.

Reddy, C. S. K., Ghai, R., Rashmi, R., & Kalia, V. C. (2003). Polyhydroxyalkanoates: An overview. *Bioresource Technology*, *87*, 137–146.

Satyanarayana, K. G., Arizaga, G. G. C., & Wypych, F. (2009). Biodegradable composites based on lignocellulosic fibers—An overview. *Progress in Polymer Science*, *34*, 982–1021.

Sgriccia, N., Hawley, M. C., & Misra, M. (2008). Characterization of natural fiber surfaces and natural fiber composites. *Composites, A: Applied Science and Manufacturing*, *39*, 1632–1637.

Shogren, R. (1997). Water vapor permeability of biodegradable polymers. *Journal of Environmental Polymer Degradation*, *5*, 91–95.

Tenenbaum, D. J. (2008). Food vs. fuel: Diversion of crops could cause more hunger. *Environmental Health Perspectives*, *116*, A254–A257.

Tian, H., Tang, Z., Zhuang, X., Chen, X., & Jing, X. (2012). Biodegradable synthetic polymers: Preparation, functionalization and biomedical application. *Progress in Polymer Science*, *37*, 237–280.

Wollerdorfer, M., & Bader, H. (1998). Influence of natural fibres on the mechanical properties of biodegradable polymers. *Industrial Crops and Products*, *8*, 105–112.

Wolf, B. (2010). Polysaccharide functionality through extrusion processing. *Current Opinion in Colloid & Interface Science*, *15*, 50–54.

Zadorecki, P., & Karnerfors, H. (1986). Cellulose fibers as reinforcement in composites: Determination of the stiffness of cellulose fibers. *Composite Science and Technology*, *27*, 291–303.